EARTHQUAKE ENGINEERING AND STRUCTURAL DYNAMICS
Earthquake Engng Struct. Dyn. 2011; **40**:1103–1121
Published online 22 November 2010 in Wiley Online Library (wileyonlinelibrary.com). DOI: 10.1002/eqe.1072

The existence of 'complete similarities' in the response of seismic isolated structures subjected to pulse-like ground motions and their implications in analysis

Nicos Makris*, †, ‡ and Michalis F. Vassiliou

Department of Civil Engineering, University of Patras, Patras GR26500, Greece

SUMMARY

In this paper the seismic response of isolated structures supported on bearings with bilinear and trilinear behavior is revisited with dimensional analysis in an effort to better understand the relative significance of the various parameters that control the mechanical behavior of isolation systems. An isolation system that consists of lead rubber bearings or of single concave spherical sliding bearings exhibits bilinear behavior; whereas, when a double concave configuration is used the behavior is trilinear. For the case of bilinear behavior it is well known that the value of the normalized yield displacement is immaterial to the response of the isolated superstructure—or, in mathematical terms, that the response of the bilinear oscillator exhibits *complete similarity* in the dimensionless yield displacement. Similarly, for the case of trilinear behavior the paper shows that the presence of the intermediate slope is immaterial to the peak response of most isolated structures—a finding that shows the response of the trilinear oscillator exhibits a complete similarity in the difference between the coefficients of friction along the two sliding surfaces as well as in the ratio of the intermediate to the final slope. This finding implies that even when the coefficients of friction of the two sliding surfaces are different, the response of isolated structures for most practical configurations can be computed with confidence by replacing the double concave spherical bearings with single concave spherical bearings with an effective radius of curvature and an effective coefficient of friction.

Received 27 October 2009; Revised 26 August 2010; Accepted 26 August 2010

KEY WORDS: seismic protection; bridges; dimensional analysis; earthquake engineering; spherical sliding bearings

INTRODUCTION

During the last three decades seismic isolation enjoyed substantial growth, major improvements in its performance and an increasing worldwide acceptance [1, 2]. Several design documents are now available that offer guidelines on how to design structures equipped with this new seismic protection technology (FEMA [3, 4], AASHTO [5], IBC [6], among others). The most widely used isolation bearings are lead rubber bearings [1, 2] and spherical sliding bearings [7–9]. Until the early years of this decade most spherical sliding bearings used involved only a single concave sliding surface, and the bilinear model was sufficient to approximate the behavior of both lead rubber and sliding spherical bearings. The only appreciable difference between the shape of the bilinear curve of the lead rubber and the sliding bearing is the size of the yield displacement, u_y.

*Correspondence to: Nicos Makris, Department of Civil Engineering, University of Patras, Patras GR26500, Greece.
†E-mail: nmakris@upatras.gr
‡Professor.

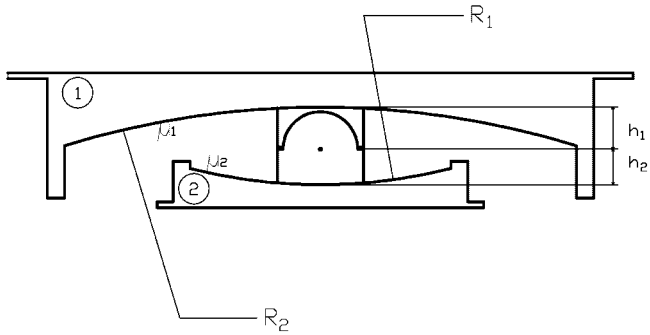

Figure 1. Cross section of a double concave spherical sliding (DCSS) bearing with different radii of curvature.

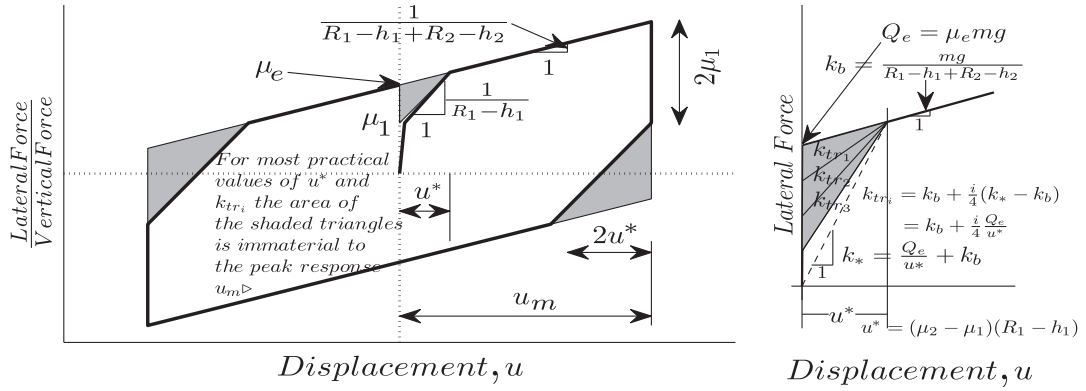

Figure 2. Left: Generic force–displacement loop of the DCSS bearing (heavy line). Right: Values of the transition slope, k_{tr}, used in this parametric study.

In the case of lead rubber bearing, u_y is of the order of centimeters ($0.01-0.03$ m) or even more; whereas, in the case of spherical sliding bearing, $u_y = 0.00025\,\text{m} = 0.25\,\text{mm}$ or even less [8, 10].

Earlier parametric studies by Makris and Chang [11] concluded that when seismic isolated structures are excited by strong ground motions, the value of the yield displacement has marginal effects on the superstructure response. This conclusion was subsequently confirmed and generalized by Makris and Black [12] via the use of dimensional analysis and it was demonstrated that the response of the bilinear oscillator exhibits complete similarity in the normalized yield displacement.

The rapid growth of seismic isolation generated the need for more compact size, large-displacement capacity, long-period bearings. Such needs are served with the double concave spherical sliding bearing—its configuration is shown schematically in Figure 1 (Hyakuda *et al.* [13], Constantinou [14], Tsai *et al.* [15], Fenz and Constantinou [16], Tsai *et al.* [17], among others). When the double concave spherical bearing has sliding surfaces with the same coefficient of friction, μ (no need for same radii of curvature) it becomes like a traditional single concave spherical bearing with isolation period $T_b = 2\pi\sqrt{(R_1+R_2-h_1-h_2)/g}$ and coefficient of friction μ.

When the coefficients of friction along the sliding interfaces are different the behavior of the double concave friction spherical bearing is trilinear and it can be modeled using two traditional single concave spherical bearings acting in series together with a point mass representing the articulated slider. With this mathematically rigorous model one can capture the shaved portions of the hysteretic loops at the initiation and at the reversal of motion (see Figure 2) when, initially, the sliding surface with the lower coefficient of friction is mobilized. Nevertheless, the implementation of two spring-slider elements in series may challenge the convergence of commercially available software which are used routinely by practitioner engineers. This convergence

DOI: 10.1002/eqe

challenge is accentuated when large structural systems are of interest such as multispan isolated bridges with isolation bearings and occasionally nonlinear dampers at the center piers and end abutments.

In this paper it is shown that when trilinear behavior prevails (see Figure 2), as it results from practical double concave spherical sliding (DCSS) bearings, the presence of the intermediate slope, k_{tr}, and the shaving of the loops when the motion reverses (which is the result of the difference in the coefficient of friction along the two interfaces) is immaterial to the response of the isolated superstructure for most practical values of the coefficients of friction used in seismic isolation of civil structures. In more rigorous mathematical terms this finding shows that the response of the trilinear oscillator exhibits *complete similarity* in the difference of the coefficient of friction along the two sliding surfaces as well as in the ratio of the intermediate to the final slope. This finding implies that under strong shaking an isolated bridge exhibits the same maximum displacement regardless of whether it is supported on a DCSS (R_1-h_1, R_2-h_2, μ_1, μ_2) or single concave (R_e, μ_e) spherical sliding (SCSS) bearing provided that

$$\frac{1}{R_e}=\frac{1}{R_1-h_1+R_2-h_2} \tag{1}$$

and

$$\mu_e=\frac{\mu_1(R_1-h_1)+\mu_2(R_2-h_2)}{R_1-h_1+R_2-h_2} \tag{2}$$

Similar results, without referring to the property of complete similarity, have been presented in a recent study [18] on double concave variable frequency sliding bearings.

The existence of this *complete similarity* has practical significance in terms of estimating peak response displacements since it eliminates the need of implementing two spring-slider elements in series and the analysis may be performed for all practical purposes with an equivalent SCSS bearing. The permanent displacement that results from the equivalent single concave spherical bearings can be either smaller or larger than that resulting from the double concave spherical bearings, depending on the ground motion.

This study is restricted to the response analysis of an isolated deck and its findings apply to the peak sliding displacement. The effect of the transition slope of the trilinear oscillator to the acceleration response of multi-degree-of-freedom isolated structures will be the subject of a future study.

PARAMETERS OF THE BILINEAR SDOF OSCILLATOR

With reference to Figure 3 (left) consider a rigid deck supported on bearings that exhibit bilinear hysteretic behavior. Additional viscous dissipation can be appended if desired. The mechanical model adopted herein has been widely used for years for the modeling of either lead rubber or SCSS bearings ([1, 2, 9, 11, 19], references reported therein) and has been systematically implemented for the response analysis of seismically isolated structures (SAP2000N, OpenSEES among other commercially available or open source software).

The bilinear model shown in Figure 3 (right) consists of the superposition of a linear restoring mechanism and some energy dissipation mechanism which is approximated with a parallelogram. In the case of frictional dissipation ($u_y=0.25$ mm [8]) the yield displacement prior to flow is small; yet the behavior remains bilinear.

The bilinear force–displacement loop shown in Figure 3 (right) is uniquely defined with the isolation frequency induced by the bearings $\omega_b=\sqrt{k_b}/m=2\pi/T_b$, the characteristic strength, Q, and the yield displacement u_y. Note that the isolation frequency, ω_b, is the undamped frequency of the mass, m, of the deck restrained by the stiffness of the bearings, $k_b=m\omega_b^2$, which is the second slope of the bilinear loop. This definition is consistent with the frequency of oscillation of isolated

DOI: 10.1002/eqe

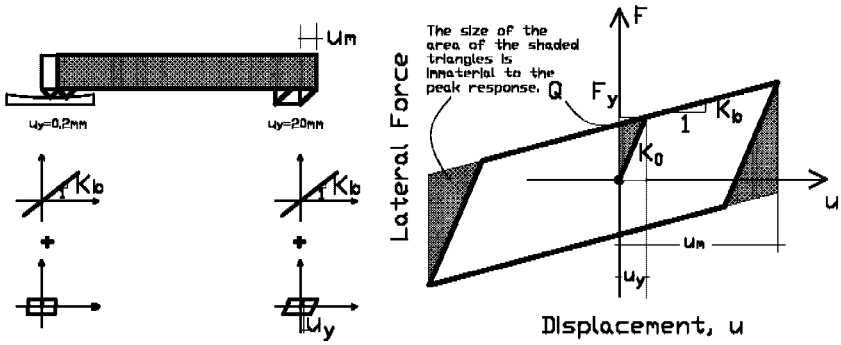

Figure 3. Left: Rigid deck isolated on bearings that exhibit bilinear behavior. Right: Generic force–displacement loop.

structures supported on single-concave friction pendulum bearings with radius of curvature R. In this case

$$\omega_b = \sqrt{\frac{k_b}{m}} = \sqrt{\frac{W}{R}\frac{1}{m}} = \sqrt{\frac{g}{R}} \tag{3}$$

The first slope K_0, of the bilinear loop

$$K_0 = \frac{Q}{u_y} + K_b \tag{4}$$

is mostly associated with the preyielding behavior of the energy dissipation mechanism and depends primarily on the value of the yield displacement u_y. Early parametric studies by Makris and Chang [11] concluded that when seismic isolated structures are excited by strong earthquakes, the value of the yield displacement has marginal effects on the superstructure response. This conclusion was subsequently confirmed and generalized by Makris and Black [12] via the use of dimensional analysis.

TIME SCALE AND LENGTH SCALE OF PULSE-LIKE GROUND MOTIONS

The dimensional analysis of the seismic response of inelastic structures requires a time scale and a length scale of the ground excitation. Such time scales and length scales are distinguishable in a wide class of strong ground motions known as 'pulse-like' ground motions most of them recorded *near the source* of causative faults.

The relative simple form, yet destructive potential of pulse-like ground motions has motivated the development of various closed-form expressions which approximate their leading kinematic characteristics. The early work of Veletsos *et al.* [20] was followed by the papers of Hall *et al.* [21], Heaton *et al.* [22], Makris [23], Makris and Chang [11], Alavi and Krawinkler [24], and more recently by the paper of Mavroeidis and Papageorgiou [25]. Some of the proposed pulses are physically realizable motions with zero final ground velocity and finite accelerations, whereas some other idealizations violate one or both of the above requirements. Physically realizable pulses can adequately describe the impulsive character of near-fault ground motions both qualitatively and quantitatively. The input parameters of the model have an unambiguous physical meaning. The minimum number of parameters is two, which are either the acceleration amplitude, a_p, and duration, T_p, or the velocity amplitude, v_p and duration, T_p [11, 23]. The more sophisticated model of Mavroeidis and Papageorgiou [25] involves four parameters, which are the pulse period, the pulse amplitude as well as the number and phase of half cycles, and was found to describe a large set of velocity pulses generated due to forward directivity or permanent translation effect. The pulse period, T_p, of the most energetic pulse of strong ground motions is strongly correlated with

DOI: 10.1002/eqe

the moment magnitude, M_w, of the event. For a given moment magnitude, the duration of pulses produced by strike-slip faults is on average larger than the duration of pulses generated by reverse faults. Assuming that the time scale T_p is independent of the source–station distance, for stations located within $\sim$10 km from the causative fault, the pulse period and moment magnitude are related through the following empirical relationship which also satisfies a self-similarity condition [25–27]:

$$\ln T_p = -2.9 + 0.5 M_w \tag{5}$$

Furthermore, seismological data indicate that the amplitude of the velocity pulses recorded within a distance of 7 km from the causative fault varies from 60 to 120 cm/s. This observation is in good agreement with the typical slip velocity value of 90 cm/s frequently considered by seismologists [28, 29].

The current established methodologies for estimating the pulse characteristics of a wide class of records are of unique value since the product, $a_p T_p^2 = L_p$, is a characteristic length scale of the ground excitation and is a measure of the persistence of the most energetic pulse to generate inelastic deformations [30]. It is emphasized that the persistence of the pulse is a different characteristic from the strength of the pulse which is measured with the peak pulse acceleration. The reader should recall that among two pulses with different acceleration amplitude (say $a_{p1} > a_{p2}$) and different pulse duration (say $T_{p1} < T_{p2}$), the inelastic deformation does not scale with the peak pulse acceleration (most intense pulse) but with the stronger length scale (larger $a_p T_p^2 =$ most persistent pulse).

The heavy line in Figure 4 (left) which approximates the long-period acceleration pulse of the NS component of the 1992 Erzinkan, Turkey, record is a scaled expression of the second derivative of the Gaussian distribution, $e^{-\frac{t^2}{2}}$, known in the seismology literature as the symmetric Ricker wavelet [31, 32] and widely referred as the 'Mexican Hat' wavelet [33]

$$\psi(t) = a_p \left(1 - \frac{2\pi^2 t^2}{T_p^2}\right) e^{-\frac{1}{2}\frac{2\pi^2 t^2}{T_p^2}} \tag{6}$$

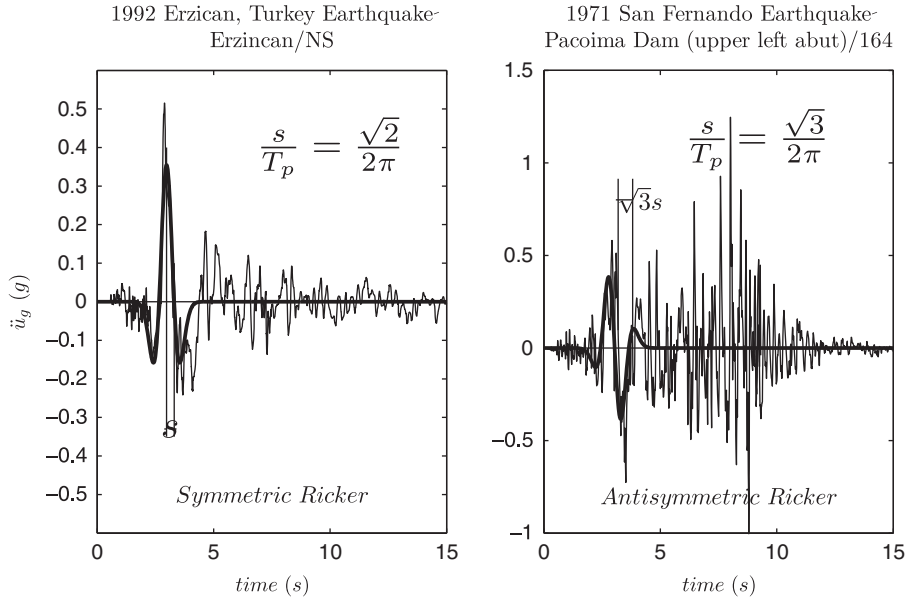

Figure 4. Left: North–South components of the acceleration time history recorded during the 1992 Erzican, Turkey earthquake together with a symmetric Ricker wavelet. Right: Fault-normal component of the acceleration time history recorded during the 1971 San Fernando earthquake, together with an antisymmetric Ricker wavelet.

DOI: 10.1002/eqe

The value of $T_p = 2\pi/\omega_p$ is the period that maximizes the Fourier spectrum of the symmetric Ricker wavelet.

Similarly, the heavy line in Figure 4 (right) which approximates the long-period acceleration pulse of the Pacoima Dam motion recorded during the February 9, 1971 San Fernando, California earthquake is a scaled expression of the third derivative of the Gaussian distribution $e^{-t^2/2}$. Again, in Equation (7) the value of $T_p = 2\pi/\omega_p$ is the period that maximizes the Fourier spectrum of the antisymmetric Ricker wavelet

$$\psi(t) = \frac{a_p}{\beta}\left(\frac{4\pi^2 t^2}{3T_p^2} - 3\right) t e^{-\frac{1}{2}\frac{4\pi^2 t^2}{3T_p^2}} \tag{7}$$

in which β is a factor equal to 1.3801 that enforces the above function to have a maximum equal to a_p.

The choice of the specific functional expression to approximate the main pulse of pulse-type ground motions has limited significance in this work. In the past, simple trigonometric pulses have been used by the senior author [11, 12, 23, 30] to extract the time scale and length scale of pulse-type ground motions. In this paper we use as alternative wavelets the symmetric and antisymmetric Ricker wavelets. A mathematically rigorous and easily reproducible methodology based on wavelet analysis to construct the best matching wavelet has been recently proposed by Vassiliou and Makris [34].

REVIEW OF DIMENSIONAL ANALYSIS OF THE BILINEAR SDOF OSCILLATOR

Consider a hysteretic bilinear oscillator that is described with the three parameters ω_b, Q/m, and u_y ($\xi = 0$), which is subjected to a pulse type strong ground motion with a predominant acceleration pulse with duration $T_p = 2\pi/\omega_p$ and amplitude a_p. With these structural and excitation parameters the maximum inelastic displacement of the bilinear SDOF oscillator is a function of five variables

$$u_{\max} = f\left(\omega_b, \frac{Q}{m}, u_y, a_p, \omega_p\right) \tag{8}$$

The six (6) variables appearing in Equation (8), $u_{\max} \doteq [\mathrm{L}]$, $\omega_b \doteq [\mathrm{T}]^{-1}$, $Q/m \doteq [\mathrm{L}][\mathrm{T}]^{-2}$, $u_y \doteq [\mathrm{L}]$, $a_p \doteq [\mathrm{L}][\mathrm{T}]^{-2}$, and $\omega_p \doteq [\mathrm{T}]^{-1}$, involve only two reference dimensions; that of length [L] and time [T]. According to Buckingham's Π-theorem the number of dimensionless products (Π-Terms) = (number of variables in Equation (8) = 6)− (number of reference dimensions = 2); therefore for the bilinear SDOF oscillators, we have $6-2=4\Pi$-terms

$$\Pi_m = \frac{u_{\max}\omega_p^2}{a_p} \tag{9}$$

$$\Pi_\omega = \frac{\omega_b}{\omega_p} \tag{10}$$

$$\Pi_Q = \frac{Q}{m a_p} \tag{11}$$

$$\Pi_y = \frac{u_y \omega_p^2}{a_p} \tag{12}$$

In deriving the Π-terms listed above we selected as repeating variables the characteristics of the pulse excitation, a_p and $\omega_p = 2\pi/T_p$. With this selection the maximum displacement response, $u_{\max}$, is normalized with the energetic length scale $L_e = a_p/\omega_p^2$ that is a measure of the persistence

DOI: 10.1002/eqe

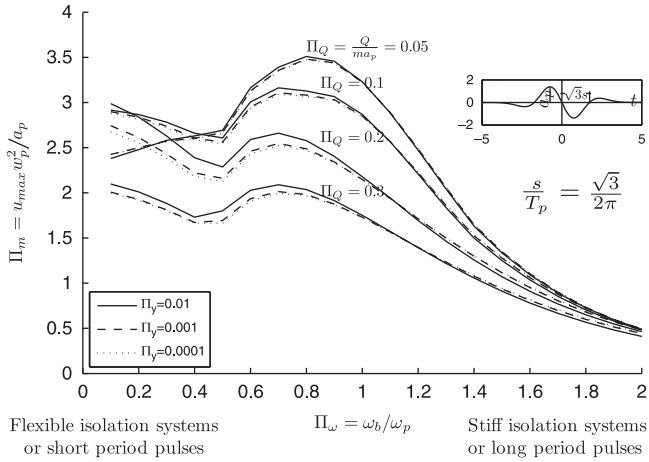

Figure 5. Dimensionless maximum displacement spectra of a bilinear oscillator subjected to an antisymmetric Ricker wavelet. For a given dimensionless strength Π_Q, the response is practically independent to 2 orders of magnitude variation of the dimensionless yield displacement Π_y.

of the excitation. With the four Π-terms given above the relation of the six variables appearing in Equation (8) is reduced to a relation of four variables

$$\frac{u_{\max}\omega_p^2}{a_p} = \varphi\left(\frac{\omega_b}{\omega_p}, \frac{Q}{ma_p}, \frac{u_y\omega_p^2}{a_p}\right) \tag{13}$$

Figure 5 plots the dimensionless value of the solution of Equation (13), $\Pi_m = u_{\max}\omega_p^2/a_p$, as a function of $\Pi_\omega = \omega_b/\omega_p$ for three different values of $\Pi_Q = Q/ma_p$ and different values of $\Pi_y = u_y\omega_p^2/a_p$, when the bilinear SDOF oscillator is excited by an antisymmetric Ricker wavelet. Figure 5 reveals two important results that emerge from the unique advantages of dimensional analysis. The first result is the result of *self similarity*—which for a given value of the dimensionless strength, Π_Q, and the dimensionless yield displacement, Π_y, the dimensionless response of the bilinear oscillator, Π_m, follows the same master curve for all values of excitation levels (any value of the pulse acceleration amplitude and pulse duration), showing that the solutions for the dimensionless peak response values are self similar. This result underlines the important physical significance of the Π-terms given by Equations (9)–(12). The second and most important result is the result of *complete similarity*—that for a given value of the dimensionless strength, Π_Q, the solution for the dimensionless maximum displacement, Π_m, is nearly independent even when the dimensionless yield displacement, Π_y, is varied by 2 orders of magnitude ($\Pi_y = 0.0001 - 0.01$). Similar spectra for trigonometric pulses have been presented by Makris and Black [12]. This finding implies that, under earthquake shaking, an isolated bridge exhibits the same maximum displacement regardless of whether it is supported on lead rubber bearings or SCSS bearings that exhibit the same strength and offer the same second slope (same isolation period). In mathematical terms, the dimensionless response Π_m, converges to a finite limit (neither zero nor infinity) as the dimensionless yield displacement Π_y tends to zero; and according to the theory of dimensional analysis one can simply replace Equation (13) by its limiting expression in which Π_y is sufficiently small and drops out of consideration [35]

$$\lim_{\Pi_y \to 0} \frac{u_{\max}\omega_p^2}{a_p} = \varphi\left(\frac{\omega_b}{\omega_p}, \frac{Q}{ma_p}, \Pi_y\right) = \text{finite} \quad \Rightarrow \quad \frac{u_{\max}\omega_p^2}{a_p} \simeq \varphi\left(\frac{\omega_b}{\omega_p}, \frac{Q}{ma_p}\right) \tag{14}$$

The finding that the response of the bilinear oscillator exhibits complete similarity in the normalized yield displacement expressed by Equation (14) is what is of most interest to the design structural engineer–that the exact value of the yield displacement, u_y, is immaterial to the response of the bilinear SDOF oscillator and therefore drops out of consideration. Furthermore, because of

DOI: 10.1002/eqe

the existence of complete similarity as expressed by Equation (14), the number of arguments in the function $\phi()$, appearing in Equation (13) reduces by one.

PARAMETERS OF THE TRILINEAR SDOF OSCILLATOR

Our study proceeds with the dimensional analysis of the dynamic response of the trilinear SDOF oscillator in an effort to better understand the relative significance of the various parameters that control the mechanical behavior of the DCSS bearing.

The DCSS bearings consist of two facing concave stainless-steel surfaces as shown in Figure 1. The top and bottom concave surfaces have radii of curvature R_1 and R_2, respectively, which may be unequal. The coefficients of friction of the concave surfaces are μ_1 and μ_2, respectively, which are also not necessarily equal. An articulated slider faced with a non-metallic sliding material separates the two surfaces. The principal benefit of the DCSS bearing is its capacity to accommodate larger displacement demands compared to the SCSS bearing examined in the previous section.

When different values of coefficients of friction are used ($\mu_1 \neq \mu_2$), the force–displacement loop of the DCSS bearing is not bilinear—as is for the SCSS bearing shown in Figure 3—but rather trilinear given that at the initiation and at the reversal of motion, the bilinear loop loses the corner triangles (see Figure 2, left) when the sliding surface with the lower coefficient of friction is mobilized.

The purpose of this section is to show that the loss of the corner triangles shown in gray in Figure 2 is immaterial in the response of the isolated superstructure for most practical values of the coefficients of friction used. In mathematical terms, the paper shows that the trilinear oscillator exhibits complete similarity in the difference between the coefficients of friction along the two sliding surfaces as well as in the ratio of the intermediate to the final slope.

The trilinear force–displacement loop shown in Figure 2 is uniquely defined with the isolation frequency offered by the bearings

$$\omega_b = \sqrt{\frac{g}{R_1 - h_1 + R_2 - h_2}} \tag{15}$$

the characteristic strength,

$$Q_e = mg\frac{\mu_1(R_1 - h_1) + \mu_2(R_2 - h_2)}{R_1 - h_1 + R_2 - h_2} \tag{16}$$

the yield displacement of the equivalent bilinear system $u_{ye} \approx 0.25\,\text{mm}$, which according to the previous analysis we expect to have marginal effect, the transition displacement from the second to the last slope,

$$u^* = (\mu_2 - \mu_1)(R_1 - h_1) \tag{17}$$

and the transition frequency associated with the second slope,

$$\omega_{\text{tr}} = \sqrt{\frac{g}{R_1 - h_1}} \tag{18}$$

In this study, while the analysis focuses on the DCSS bearings the formulation is presented for the general trilinear oscillator ($u_{ye} \neq 0$) and the result that the normalized maximum displacement exhibits a complete similarity in the normalized yield displacement is re-established.

PARAMETRIC ANALYSIS OF THE RESPONSE OF AN ISOLATED DECK ON DCSS BEARINGS

Our parametric analysis to investigate the relative significance of the various parameters that control the mechanical behavior of the DCSS bearings commences with the response analysis of

DOI: 10.1002/eqe

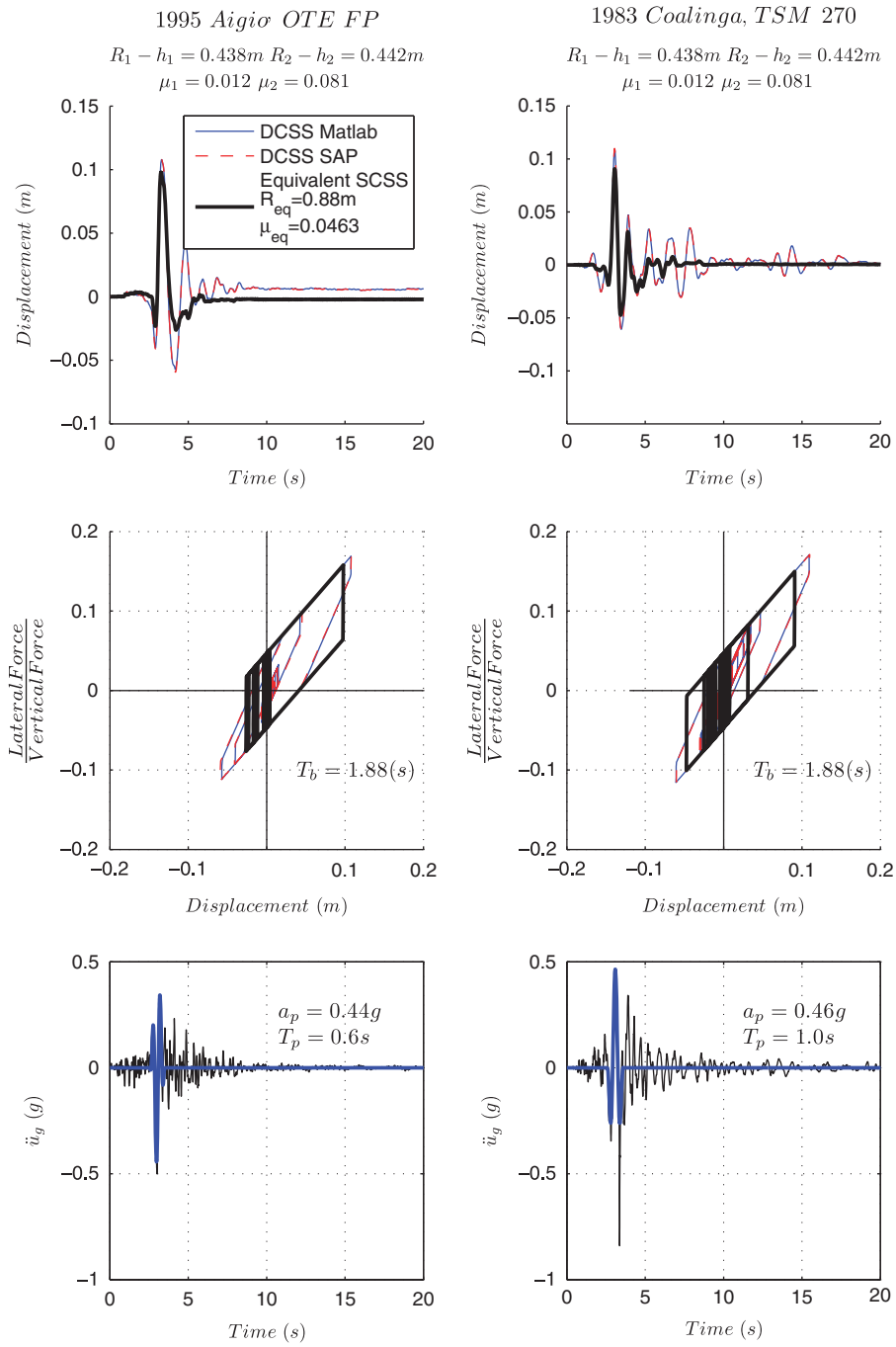

Figure 6. Comparison of displacement time histories (top) and force–displacement loops (center) of a rigid deck isolated on double concave spherical sliding bearings (DCSS) bearings and on the equivalent SCSS bearing when subjected to the OTE FP acceleration record from the 1995 Aigion (left) and to the TSM270 acceleration record from the Coalinga 1983 earthquake (right).

a rigid isolated deck that is supported on DCSS bearings. Figure 6 plots the relative-to-the-ground deck displacement (bearing displacement) when the structure is subjected to the fault-parallel OTE record from the $M_w = 6.2$, 1995 Aigion, Greece earthquake (left); and to the Transmitter Hill 270 record from the Mw = 5.8, 1983 Coalinga earthquake (right). The double concave spherical bearing used is the one tested by Fenz and Constantinou [16]—the configuration with the

DOI: 10.1002/eqe

largest difference in the coefficient of friction ($\mu_1=0.012$, $\mu_2=0.081$, $R_1-h_1=0.438\,\text{m}$, $R_2-h_2=0.442\,\text{m}$, $u^*=(\mu_2-\mu_1)(R_1-h_1)=0.03\,\text{m}=3\,\text{cm}$). For the moderately strong OTE FP record of the 1995 Aigion earthquake ($a_p=0.44\,\text{g}$ and $T_p=0.60\,\text{s}$), the peak sliding displacement is $u_m=9.8\,\text{cm}$ when the SCSS bearing is used and $u_m=10.7\,\text{cm}$ when the DCSS bearings are used. Accordingly, in this case where u^* is as large as 30% of u_m, the difference in the peak sliding displacement between the DCSS and SCSS bearings is $10.7\,\text{cm}-9.8\,\text{cm}=0.9\,\text{cm}$. Now this 0.9 cm difference is 9% of the peak sliding displacement (and may not be negligible to someone); however, because the peak sliding displacement is small, this 9% difference $=0.9\,\text{cm}$ is 'immaterial' in the seismic response analysis of the isolated structure in terms of peak design quantities. (even these smaller bearings used in Figure 6, which offer an isolation period of $T_b=1.88\,\text{s}$, have a displacement capacity $=15.3\,\text{cm}$.) For the Transmitter Hill record a similar behavior is observed.

The response analysis presented in Figure 6 has been computed with an in-house MATLAB code (solid line) and with the SAP software (dashed lines) by connecting two spring-slider elements in series. The numerical result of the two calculations shown both on the displacement time histories and the force displacement loops are identical and this validates the solution obtained with SAP.

Returning to Figure 6 (left) the response analysis with the equivalent SCSS bearings results to zero-permanent displacement; whereas the response analysis with the DCSS bearing reaches a small permanent displacement due to the high friction $\mu_2=0.081$ on surface one. This result is not a general trend given that the opposite may happen depending on the fluctuations of the ground excitation that follow the main pulse.

DIMENSIONAL ANALYSIS OF THE TRILINEAR OSCILLATOR

Consider a trilinear oscillator that is described with the five parameters ω_b, Q_e, u_{ye}, u^*, and ω_{tr} which is subjected to a pulse-type strong ground motion having a predominant acceleration pulse with duration T_p and amplitude a_p. The maximum inelastic displacement of the trilinear SDOF oscillator is a function of seven variables

$$u_{\max}=f\left(\omega_b,\frac{Q_e}{m},u_{ye},u^*,\omega_{\text{tr}},a_p,\omega_p\right) \tag{19}$$

The eight (8) variables appearing in Equation (19) involve only two reference dimensions that of length [L] and time [T]. According to Buckingham's Π-theorem, the number of dimensionless products (Π-terms) = (number of variables in Equation (19) = 8 – number of reference dimensions = 2); therefore, for the trilinear SDOF oscillator we have $8-2=6\Pi$-terms. The first two Π-terms (Π_m and Π_ω) are given by Equations (9) and (10) while,

$$\Pi_Q=\frac{Q_e}{ma_p} \tag{20}$$

$$\Pi_y=\frac{u_{ye}\omega_p^2}{a_p}\neq 0 \tag{21}$$

$$\Pi_*=\frac{u^*\omega_p^2}{a_p} \tag{22}$$

$$\Pi_{tr}=\frac{\omega_{\text{tr}}}{\omega_p} \tag{23}$$

As in the dimensional analysis of the bilinear oscillator in deriving the Π-terms listed above we selected as repeating variables the characteristics of the pulse excitation, a_p and $\omega_p=2\pi/T_p$. With the six Π-terms given by Equations (9), (10), (20)–(22), the relation of the eight variables

DOI: 10.1002/eqe

appearing in Equation (19) is reduced to a relation of six variables

$$\frac{u_{\max}\omega_p^2}{a_p}=\varphi\left(\frac{\omega_b}{\omega_p},\frac{Q_e}{ma_p},\frac{u_{ye}\omega_p^2}{a_p},\frac{u^*\omega_p^2}{a_p},\frac{\omega_{\mathrm{tr}}}{\omega_p}\right) \tag{24}$$

Range of interest of the Π*-terms*

- $\Pi_\omega=\omega_b/\omega_p$
  Given that the majority of isolation periods used are larger than 1.5 s ($T_p>1.5$ s) and that energetic pulses from near source records can be as large as 3 s, the range of interest for ω_b/ω_p is $0<\omega_b/\omega_p=T_p/T_b<3\,\mathrm{s}/1.5\,\mathrm{s}=2$. Beyond the value of $\Pi_\omega=\omega_b/\omega_p=2$ the phenomenon of complete similarity that we intend to show becomes even stronger.
- $\Pi_Q=Q_e/ma_p$
  Even for ground motions which are approximated with low amplitude acceleration pulses say $a_p=0.25$ g and for an equivalent coefficient of friction as high as $\mu_e=0.05$ the dimensionless product $\Pi_Q=Q_e/ma_p=\mu_e g/a_p$ is as high as 0.2. Accordingly $0.05<\Pi_Q<0.2$. For instance with the value of $\mu_e=0.0467$ associated with the bearing tested in Figure 6 and for the 1995 Aigion record ($a_p=0.44$ g) shown at the left of Figure 6, $\Pi_Q=0.0467/0.44=0.106$; while for the TSM270 record from the 1983 Coalinga Earthquake ($a_p=0.46$ g) shown at the right of Figure 6, $\Pi_Q=0.0467/0.46=0.102$.
- $\Pi_y=u_{ye}\omega_p^2/a_p$
  Given that the yield displacement of the Teflon coat before sliding along the stainless steel surface is $u_y=0.2$ m and that u_{ye} is of the same order of magnitude, the range of interest of $\Pi_y=u_{ye}\omega_p^2/a_p$ is $0.0001<\Pi_y<0.01$.
- $\Pi^*=u^*\omega_p^2/a_p=(\mu_2-\mu_1)(R_1-h_1)\omega_p^2/a_p$
  The main motivations/targets for developing the DCSS bearings are: (a) the need for a more compact size, large-displacement capacity sliding bearings, (b) engagement of sliding during moderate shaking, and (c) better re-centering capabilities at the weak tale-end of the excitation. Accordingly, we examine the typical values of $u^*=(\mu_2-\mu_1)(R_1-h_1)$. Table I below summarizes the values of u^* that correspond to all the configurations of DCSS bearings reported in the pertinent literature.

In order to achieve (b), the value of the coefficient of friction, μ_1, of the first sliding surface is relatively low. For instance all the values of μ_1 reported in the work of Constantinou and co-workers [14, 16] are below 4.5%. On the other hand, the values of μ_2 shall not be too high,

Table I. Selected geometrical and physical properties of DCSS bearings presented in the literature.

	Configuration	$R_1-h_1(m)$	$R_2-h_2(m)$	μ_1	μ_2	T_b(s)	u^*(m)
Fenz and Constantinou [16]	1	1.000	3.000	0.030	0.060	4.012	0.030
	2	0.442	0.438	0.012	0.081	1.882	0.030
	3	0.442	0.438	0.021	0.038	1.882	0.008
	4	0.442	0.726	0.021	0.038	2.168	0.008
Constantinou report [14]	5	2.134	2.134	0.045	0.055	4.144	0.021
	6	0.991	3.048	0.030	0.060	4.032	0.030
	7	0.442	0.438	0.017	0.055	1.882	0.017
Kim and Yun [36]	8	0.636	1.060	0.050	0.135	2.613	0.054
	9	0.420	1.130	0.060	0.115	2.498	0.023
	10	0.559	0.994	0.050	0.128	2.500	0.044
	11	0.718	0.832	0.070	0.126	2.498	0.040
	12	0.994	0.559	0.050	0.189	2.500	0.138
Parametric analysis of this study on a three span bridge	Case 1	1.100	1.100	0.030	0.060	2.975	0.033
	Case 2	1.100	1.100	0.020	0.070	2.975	0.055
	Case 3	0.700	1.500	0.010	0.063	2.975	0.037

DOI: 10.1002/eqe

because this will result into sticking of the top larger-radius surface (permanent displacement) even if the bottom smaller-radius surface re-centers. For instance, the value of μ_2 reported in the work of Constantinou and co-workers [14, 16] for long period bearings ($T_b \approx 4.0$ s) is 6%; and the largest value reported in the same work for $\mu_2 - \mu_1 = 0.03$. In the parametric-analysis paper of Kim and Yun [36] who investigated shorter period isolation systems ($T_b \approx 2.5$ s) the value of μ_2 reached or exceeded 12%; however, the values of $\mu_2 - \mu_1$ were of the order of 6%—that is two times the peak value of $\mu_2 - \mu_1 = 0.03$ used by Constantinou and co-workers [14, 16].

Now, in order to achieve (c), the stiffness that corresponds to the first sliding surface is steep; therefore, the value of the radius of curvature, $R_1 - h_1$ has to be kept small. Note that in Table I the values of $R_1 - h_1$ of all configurations, where the two sliding surfaces have different curvatures, are below 1.0 m. It is acknowledged that some of the configurations listed in Table I are small-size bearings (small $R_1 - h_1$) which have been primarily developed for experimental testing (those which are shaded), nevertheless, the resulting isolation period $T_b = 1.88$ s is large enough to qualify for selected real-world implementations.

Accordingly, it is because of this governing need to achieve re-centering under weak excitations (stiffness not too low and friction not too high), that the value of $u^* = (\mu_2 - \mu_1)(R_1 - h_1)$ in most practical cases is less than $0.06\,\text{m} \times 1.0\,\text{m} = 0.06\,\text{m}$ (see values of u^* for each configuration in Table I—all of them are below 0.055 m).

Now the stronger the acceleration pulse (larger a_p and longer duration; therefore, smaller ω_p), the smaller the value of Π^*. For instance, the six stronger out of the seven pulse-like ground motions listed in Table III of the paper exhibit an inverse length scale $= \omega_p^2/a_p < 10\,\text{m}^{-1}$. Given that Table I indicates that all practical values of $u^* = (\mu_2 - \mu_1)(R_1 - h_1)$ are less than 0.06 m so that all practical values of $\Pi^* = u^* \omega_p^2/a_p$ are below $0.06\,\text{m} \times 10\,\text{m}^{-1} = 0.6$. In order to cover other less common situations we extended the upper value of $\Pi^* = u^* \omega_p^2/a_p$ up to one ($\Pi^* \leqslant 1.0$). Thus according to the above discussion, the range $0 < \Pi^* \leqslant 1.0$ covers most practical combinations of DCSS bearings in association with pulse characteristics of 'pulse-like' strong ground motions.

- $\Pi_{\text{tr}} = \omega_{\text{tr}}/\omega_p$

With reference to Figure 2 (right) the transition slope k_{tr} (second slope) is bounded by $k_b < k_{\text{tr}} < \frac{Q_e}{u^*} + k_b = k^*$. Accordingly, in terms of frequencies

$$\omega_b < \omega_{\text{tr}} < \sqrt{\frac{Q_e}{mu^*} + \omega_b^2} \tag{25}$$

Recognizing that $\frac{Q_e}{mu^*} = \frac{\Pi_Q}{\Pi^*}\omega_p^2$, Equation (25) after dividing with ω_p assumes the expression

$$\Pi_\omega < \Pi_{\text{tr}} < \sqrt{\frac{\Pi_Q}{\Pi^*} + \Pi_\omega^2} \tag{26}$$

The limiting value of $\Pi_{\text{tr}} = \sqrt{\frac{\Pi_Q}{\Pi^*} + \Pi_\omega^2}$ is the normalized slope that corresponds to a zero coefficient of friction along one sliding surface (say $\mu_1 = 0$). In our parametric study we consider the upper value of Π_{tr} equal to $\sqrt{\Pi_\omega^2 + \frac{3}{4}\frac{\Pi_Q}{\Pi^*}}$. Accordingly,

$$\Pi_\omega^2 < \Pi_{\text{tr}}^2 < \Pi_\omega^2 + \frac{3}{4}\frac{\Pi_Q}{\Pi^*} \Rightarrow \Pi_\omega < \Pi_{\text{tr}} < \sqrt{\Pi_\omega^2 + \frac{3}{4}\frac{\Pi_Q}{\Pi^*}} \tag{27}$$

Complete similarity on the dimensionless yield displacement

Figure 7 plots the dimensionless value of the solution of Equation (24), $\Pi_m = u_{\max}\omega_p^2/a_p$ as a function of $\Pi_\omega = \omega_b/\omega_p$ when $\Pi^* = 0.5$ and $\Pi_{\text{tr}} = \sqrt{\Pi_\omega^2 + (1/2)\Pi_Q/\Pi^*}$, for three different values $\Pi_Q = Q_e/ma_p$ and different values of $\Pi_{ye} = u_{ey}\omega_p^2/a_p$ when the trilinear oscillator (rigid deck supported on DCSS bearings) is excited by an antisymmetric Ricker wavelet. Figure 7 shows that the solution for the dimensionless maximum displacement, Π_m, is nearly indifferent even when

DOI: 10.1002/eqe

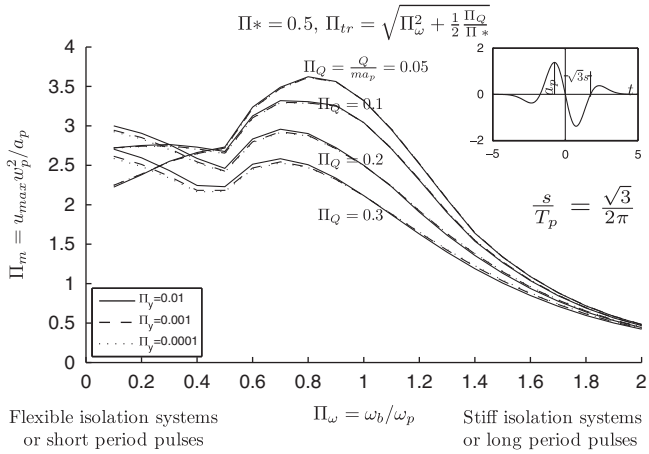

Figure 7. Dimensionless maximum displacement spectra of a trilinear oscillator ($\Pi^* = 0.5, \Pi_{\text{tr}} = \sqrt{\Pi_\omega^2 + (1/2)\Pi_Q/\Pi^*}$) subjected to an antisymmetric Ricker wavelet. For a given dimensionless strength Π_Q the response is practically indifferent to 2 orders of magnitude variation of the dimensionless yield displacement Π_y.

the dimensionless yield displacement of the backbone curve Π_y is varied by 2 orders of magnitude ($\Pi_y = 0.0001 - 0.01$). This result indicates that the response of the trilinear oscillator exhibits complete similarity in the dimensionless product Π_y, and therefore the dimensionless product Π_y drops out of consideration. Accordingly, Equation (24) reduces to

$$\frac{u_{\max}\omega_p^2}{a_p} = \varphi\left(\frac{\omega_b}{\omega_p}, \frac{Q_e}{ma_p}, \frac{u^*\omega_p^2}{a_p}, \frac{\omega_{\text{tr}}}{\omega_p}\right) \tag{28}$$

It is worth mentioning that the work of Constantinou [14] and subsequently the work of Fenz and Constantinou [16, 37] silently use the result of Equation (28)—that the response is insensitive to the value of the yield displacement and throughout their study they adopted $u_{ye} = 0$.

Interpretation of the response analysis of the DCSS bearings

Figure 8 plots dimensionless response spectra of the trilinear oscillator for three values of the normalized strength $\Pi_Q = Q_e/ma_p = \mu_e g/a_p = 0.05$, 0.1, and 0.2 when subjected to a symmetric Ricker wavelet (see Equation (6) and Figure 4). The heavy black line plots the response of the rigid deck when supported on equivalent SCSS bearings (backbone curve) while the other curves plot the response of the rigid deck supported on various DCSS bearings ($\Pi^* = 0.1, 0.5, 1.0$) and $\Pi_{\text{tr}} = \sqrt{\Pi_\omega^2 + j\Pi_Q/\Pi^*}$, $\quad j = \frac{1}{4}, \frac{1}{2}, \frac{3}{4}$, a total of nine combinations). The combination of $\Pi^* = 1.0$ and $\Pi_{\text{tr}} = \sqrt{\Pi_\omega^2 + (3/4)\Pi_Q/\Pi^*}$ corresponds to the triangles with the larger area (larger departure from the backbone loop, see Figure 2). Figure 8 indicates that the backbone heavy black line (deck on equivalent SCSS bearings) is invariably below all curves (smaller peak bearing displacements). For the case of $\Pi_Q = 0.05$ and $\Pi_Q = 0.1$ (which is the majority of practical situations), the peak bearing displacements from all configurations are practically the same (complete similarity) for $\Pi_\omega < 0.5$ and $\Pi_\omega > 1$ while within the range $0.5 < \Pi_\omega < 1$ the response curves exhibit a mild amplification as the size of the gray triangles in Figure 2 increases.

The right plot shown in Figure 8 which is for the high-end values of the dimensionless strength $\Pi_Q = Q_e/ma_p = \mu_e g/a_p = 0.2$, indicates that the complete similarity appears in the range of interest ($\Pi_\omega < 1.5$) only when $\Pi^* < 0.5$ and $\Pi_{\text{tr}} < \sqrt{\Pi_\omega^2 + (1/2)\Pi_Q/\Pi^*}$.

Figure 9 plots dimensionless response spectra of the trilinear oscillator when subjected to an antisymmetric Ricker wavelet. The response spectra in Figure 9 exhibit remarkable order and

DOI: 10.1002/eqe

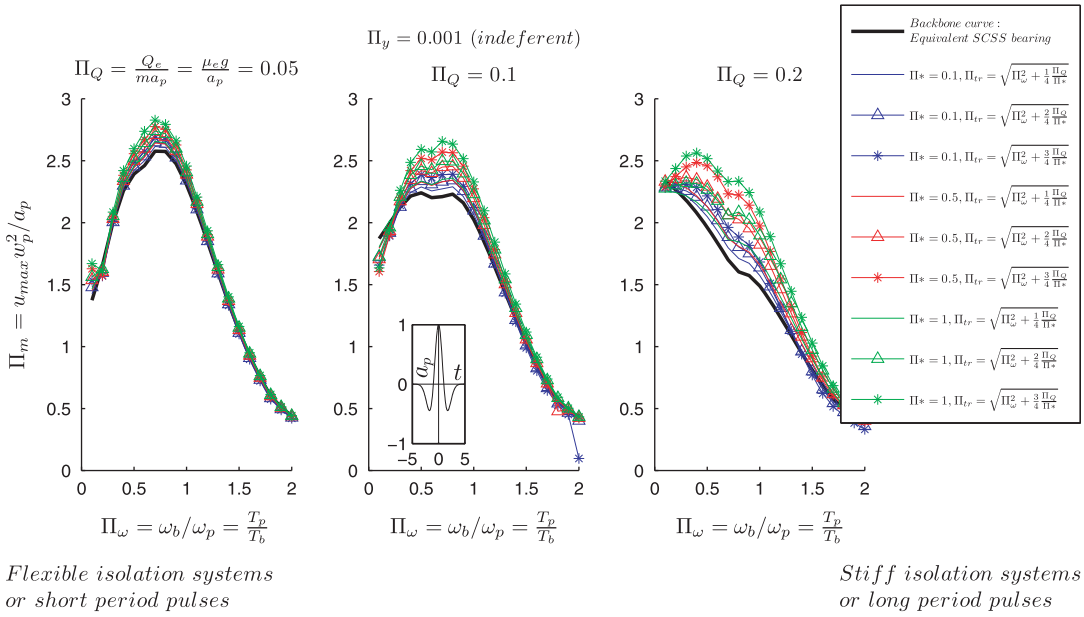

Figure 8. Dimensionless maximum inelastic displacement of a rigid deck supported on DCSS bearings with a wide range of parameters when subjected to a symmetric Ricker pulse.

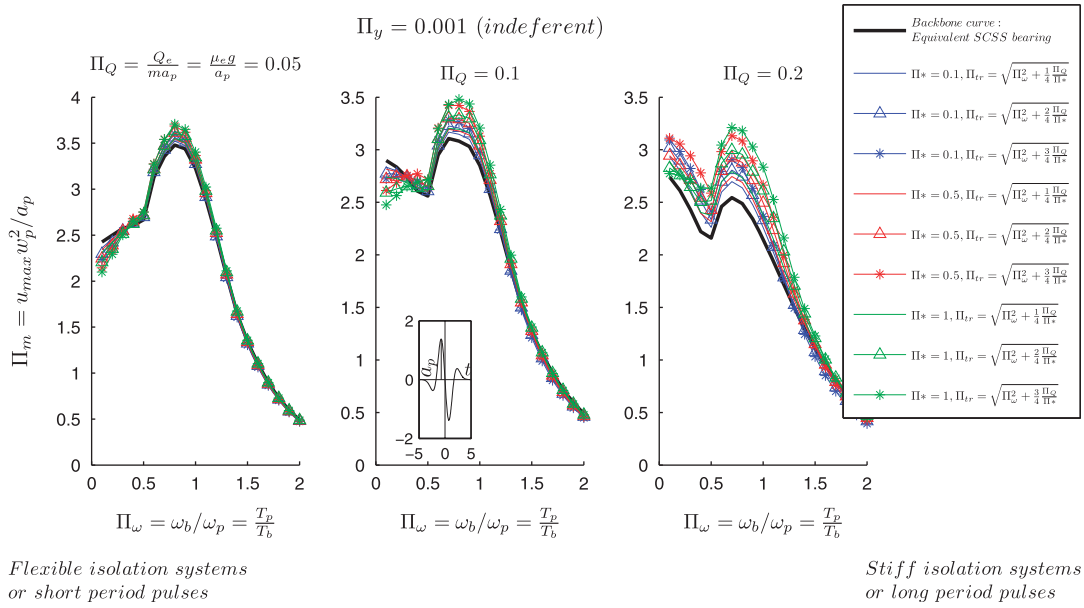

Figure 9. Dimensionless maximum inelastic displacement of a rigid deck supported on DCSS bearings with a wide range of parameters when subjected to an antisymmetric Ricker pulse.

the phenomenon of complete similarity becomes most apparent in particular for the values of $\Pi_Q < 0.1$. Also note that the curves which depart the most from the heavy black backbone line are those with the stars (*) which correspond to very high values of the transition slope ($\Pi_{tr} = \sqrt{\Pi_\omega^2 + (3/4)\Pi_Q/\Pi^*}$).

Accordingly, for values of $\Pi_Q \leqslant 0.1$ and values of $\Pi_{tr} \leqslant \sqrt{\Pi_\omega^2 + (1/2)\Pi_Q/\Pi^*}$ the response of the trilinear oscillator exhibits a complete similarity in the difference between the coefficients of

DOI: 10.1002/eqe

friction ($\Pi^* = (\mu_2 - \mu_1)(R_1 - h_1)\omega_p^2/a_p$) along the sliding interfaces as well as in the ratio of the intermediate (transition) to the final slope $\Pi_{tr} = \omega_{tr}/\omega_p$. The result of the dimensional analysis presented herein concludes that for values of $\Pi_Q \leqslant 0.1$ and values of $\Pi_{tr} < \sqrt{\Pi_\omega^2 + (1/2)\Pi_Q/\Pi^*}$ the dimensionless products Π^* and Π_{tr} drop out of consideration; and therefore Equation (28) further reduces to

$$\frac{u_{max}\omega_p^2}{a_p} = \varphi\left(\frac{\omega_b}{\omega_b}, \frac{Q_e}{ma_p}, 0, \text{any}\right) \Rightarrow \frac{u_{max}\omega_p^2}{a_p} = \varphi\left(\frac{\omega_b}{\omega_b}, \frac{Q_e}{ma_p}\right) \tag{29}$$

The finding that the response of the trilinear oscillator exhibits complete similarity in the normalized yield displacement, Π_y, in the difference between the coefficient of friction, Π^*, and the ratio of the transition to the final slope, Π_{tr}, is what is of most interest to the design structural engineer. For instance, in some cases DCSS are viable alternatives due to space limitation; however, the coefficient of friction may be different due to various imperfections. The analysis presented in this paper shows that these imperfections are immaterial to the response and one can use with confidence the equivalent values of the SCSS bearings. Furthermore, because of the existence of the three complete similarities as expressed by Equations (28) and (29) the number of arguments in the function $\phi()$ appearing in Equation (24) are reduced by three (3).

CASE-STUDY: RESPONSE OF AN ISOLATED BRIDGE

Our study to better understand the relative significance of the various parameters that control the mechanical behavior of the DCSS bearings proceeds with the response analysis of a seismically isolated bridge currently under construction in Greece in order to confirm the validity of Equation (29). This case study, is a three-span, 105-m-long seismic isolated prestressed concrete bridge supported on two piers and two end abutments. The center span is 40 m long; while the two end spans are 32.5 m long. The two piers, M1 and M2, have respective height of 11.72 m and 6.77 m and they rest in pile foundations. Figure 10 shows the elevation of the bridge. At each end-abutment or pier the bridge rests on two SCSS bearings with radius of curvature $R = 2.2$ m and coefficient of friction $\mu = 0.045$. The isolation period of the spherical bearings alone in any horizontal direction is $T_b = 2\pi\sqrt{R/g} = 2.98$ s. At the end-abutments the bridge is free to move only along the longitudinal direction, while the motion along the transverse direction is restrained in order to avoid misalignment of the rails at the deck abutment joint during earthquake shaking.

A detailed structural model of the bridge was developed with the commercially available software SAP (Computers and Structures 2007) which accounts for the flexure of the center piers and the finite stiffness of pile foundations in the horizontal, vertical, rocking, and cross horizontal-rocking directions [38].

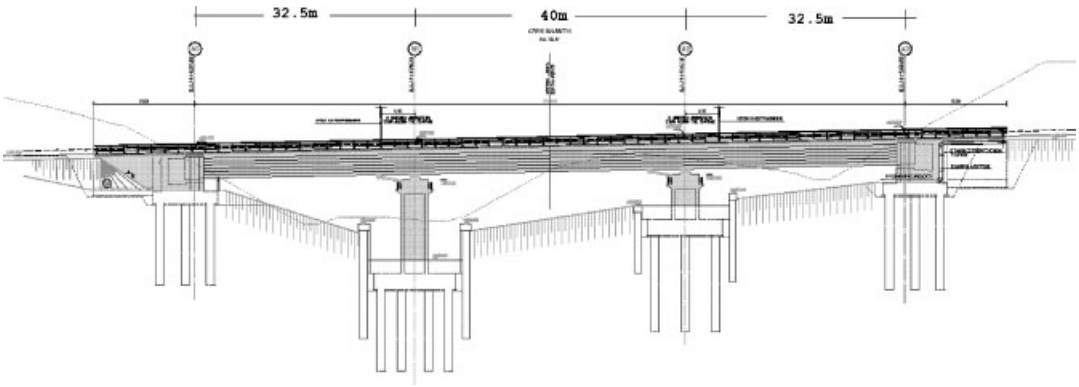

Figure 10. Elevation of a three-span, 105-m-long, seismically isolated bridge.

DOI: 10.1002/eqe

Table II. Eigenperiods of the isolated bridge shown in Figure 10.

	Eigenperiods T (s), $E_p/E_s=100$			
Modes	Equivalent SCSS bearing R_e=2.2 m μ_e=0.045	DCSS bearing Case 1 R_1-h_1=1.1 m μ_1=0.03 R_2-h_2=1.1 m μ_2=0.06	DCSS bearing Case 2 R_1-h_1=1.1 m μ_1=0.02 R_2-h_2=1.1 m μ_2=0.07	DCSS bearing Case 3 R_1-h_1=0.7 m μ_1=0.01 R_2-h_2=1.5 m μ_2=0.0613
1	2.993	2.993	2.993	2.993
2	1.007	1.007	1.007	1.007
3	0.339	0.339	0.339	0.339
4	0.290	0.290	0.290	0.290
5	0.267	0.267	0.267	0.267
6	0.193	0.193	0.193	0.193
7	0.191	0.191	0.191	0.191
8	0.152	0.152	0.152	0.152

Table III. Earthquake records used for the dynamic response analysis of the bridge.

				Longitudinal bridge direction				
Earthquake	Record station	Magnitude (Mw)	Distance (km)	PGA (g)	PGV (m/s)	$a_p(g)$	T_p(s)	$\omega_p^2/a_p(\mathrm{m}^{-1})$
1971 San Fernando	Pacoima Dam 164	6.6	11.9	1.23	1.13	0.30	1.35	7.36
1977 Bucharest		7.2	160	0.20	0.74	0.20	2.20	4.16
1979 Imperial Valley	El Centro #7/140	6.5	30	0.34	0.48	0.27	1.30	8.82
1983 Coalinga	Transmitter Hill/270	5.8	6	0.84	0.44	0.46	1.00	8.75
1986 North Palm Springs	North Palm Springs 210	6.0	8.2	0.59	0.73	0.30	1.30	7.94
1992 Erzican	Erzincan/NS	6.9	13	0.52	0.84	0.32	2.00	3.14
1996 Aigio	OTE Building/FN	6.2	20	0.50	0.43	0.44	0.60	25.41

Table II shows the first eight eigenvalues of the seismic isolated bridge shown in Figure 10 for the case where $E_p/E_s=100$ (E_p = Young's modulus of pile = 25 GPa for the concrete used and E_s = Young's modulus of soil). The first eigenvalue of the bridge is the longitudinal eigenvalue, $T_1=T_L=2.993$ s a value that is slightly larger than the SCSS bearing period, $T_b=2\pi\sqrt{R/g}=2.98$ due to the finite stiffness of the piers and piles connected in series with the spherical sliding bearings (see Figure 10).

The dynamic analysis of the bridge is also conducted by considering three configurations of DCSS bearings that offer the same isolation period and the same equivalent strength. The first configuration (Case 1) uses DCSS bearings having the same radii ($R_1-h_1=R_2-h_2=1.1$ m) and coefficient of friction $\mu_1=0.03$ and $\mu_2=0.06$ so that according to Equation (2) $\mu_e=(\mu_1+\mu_2)/2=0.045$. The second configuration (Case 2) uses DCSS bearings with $R_1-h_1=R_2-h_2=1.1$ m, and coefficients of friction further apart ($\mu_1=0.02$ and $\mu_2=0.07$).

The third configuration (Case 3) uses DCSS bearings with $R_1-h_1=0.7$ m, $\mu_1=0.01$, and $R_2-h_2=1.5$ m, $\mu_2=0.0613$. Table II, next to the eigenvalues of the bridge obtained with the SCSS bearings ($R=2.2$ m, $\mu=0.045$), offers the eignevalues computed with the three configurations of DCSS bearings described above. For all four configurations, Table II shows that the computed eigenperiods are identical.

Our study proceeds with a three-dimensional nonlinear time history analysis of the bridge shown in Figure 10 when subjected to the seven (7) ground motions (two-dimensional excitation) listed in Table III. Note that two of the seven earthquakes used (1983 Coalinga and 1995 Aigion) are moderately strong earthquakes with moderate displacement demands ($u_{\max}\approx 0.1$ m).

DOI: 10.1002/eqe

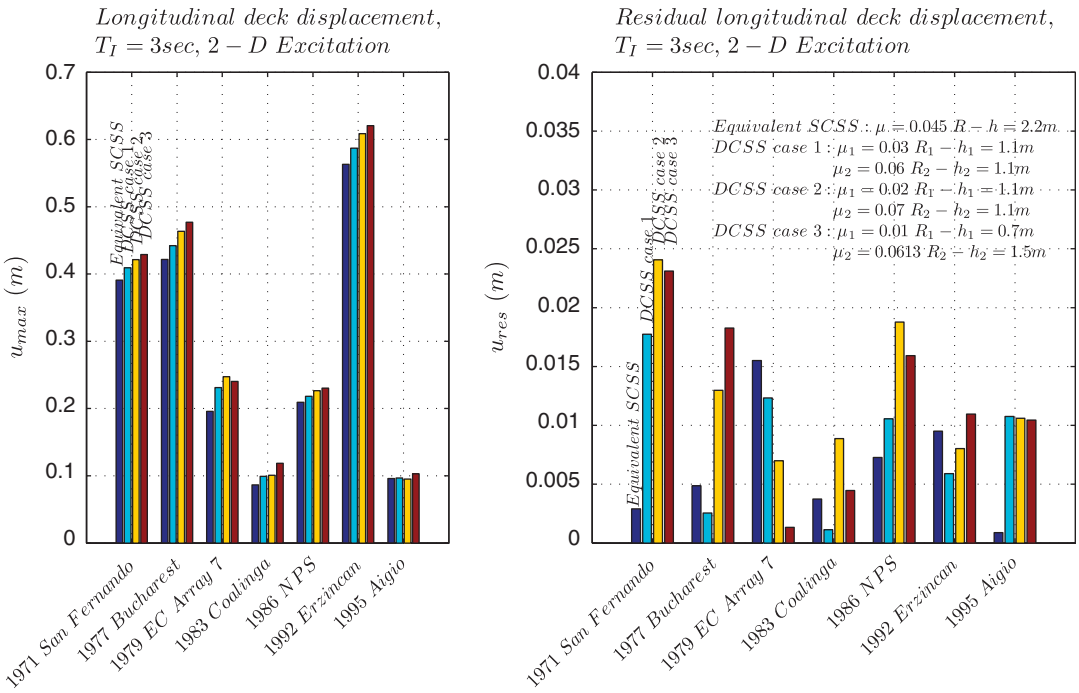

Figure 11. Comparison of peak inelastic deck displacements (top) and residual displacements (bottom) along the longitudinal direction when the bridge shown in Figure 10 is equipped with three different configurations of spherical bearings that offer the same equivalent friction and same isolation periods.

The computed response is summarized in Figure 11 which plots maximum longitudinal deck displacement (top) and residual longitudinal displacement (bottom). Figure 11 shows that for the four configurations under investigation the maximum longitudinal displacement for each ground motion are nearly the same. Accordingly, the design engineers can use with confidence the equivalent SCSS bearing for any analysis relevant to the design needs. Equally interesting are the results on the permanent displacements of the bearings where the results are mixed without exhibiting any particular trend.

CONCLUSIONS

In this paper the seismic response of isolated structures supported on bearings with bilinear and trilinear behavior is revisited with dimensional analysis in an effort to better understand the relative significance of the various parameters that control the mechanical behavior of isolated systems.

The paper introduces the concept of complete similarity by showing that the dimensionless maximum response of both bilinear and trilinear systems exhibit complete similarity in the dimensionless yield displacement. Given that the DCSS bearings may be a viable alternative due to installation limitations, the paper proceeds with a wide parametric analysis on the response of bridge decks isolated on DCSS bearings and concludes that for sufficiently small values of $\Pi^* = u^* \omega_p^2 / a_p$ (say $\Pi^* < 1.0$) and for values of the dimensionless strength $\Pi_Q = Q_e \omega_p^2 / a_p < 0.1$ and values of the dimensionless transition slope $\Pi_{\text{tr}} = \omega_{\text{tr}} / \omega_p < \sqrt{\Pi_\omega^2 + (1/2)\Pi_Q / \Pi^*}$ the response of the trilinear system exhibits complete similarity in the difference between the coefficients of friction along the sliding surface as well as in the ratio of the transition (intermediate) to the final slope. These results are restricted to the peak inelastic displacement.

The finding that for most practical configurations and design ground motions the peak response of the trilinear oscillator exhibits complete similarity in (a) the normalized yield displacement,

DOI: 10.1002/eqe

(b) the difference between the coefficient of friction, and (c) the ratio of the intermediate (transition) to the final slope is of great interest to the design engineer since the peak response of a structure isolated with DCSS bearings can be computed with confidence by using the equivalent properties of the SCSS bearings.

ACKNOWLEDGEMENTS

Partial financial support has been provided by the EU research project 'DARE' ('Soil-Foundation-Structure Systems Beyond Conventional Seismic Failure Thresholds: Application to New or Existing Structures and Monuments'), which is funded through the Seventh Framework Programme 'Ideas', Support for Frontier Research—Advanced Grant, under contract number ERC-2-9-AdG 228254-DARE.

Partial financial support has been provided to the second author by the Alexander S. Onassis Public Benefit Foundation.

REFERENCES

1. Skinner RI, Robinson WH, McVerry GH. *An Introduction to Seismic Isolation*. Wiley: Chichester, U.K., 1993.
2. Kelly JM. *Earthquake Resistant Design with Rubber*. Springer: London, 1997.
3. Federal Emergency Management Agency (FEMA). NEHRP guidelines for the seismic rehabilitation of buildings. *Report No. FEMA-273* (*Guidelines*) *and Report No. FEMA-274* (*Commentary*), Washington, DC, 1997.
4. Federal Emergency Management Agency (FEMA). Prestandard and commentary for the seismic rehabilitation of buildings. *Report No. FEMA-356*, Washington, DC, 2000.
5. AASHTO. *Guide Specifications for Seismic Isolation Design*. American Associate of State Highway and Transportation Officials, Washington, DC, 1999.
6. International Code Council (ICC). *International Building Code*, 2000.
7. Zayas VA, Low SS, Mahin SA. The FPS earthquake resisting system experimental report. *EERC Technical Report*, UBC/EERC-87/01, 1987.
8. Constantinou MC, Mokha AS, Reinhorn AM. Teflon bearing in base isolation. II: modeling. *Journal of Structural Engineering* (ASCE) 1990; **116**:455–474.
9. Constantinou MC, Soong TT, Dargush GF (eds). Passive energy dissipation systems for structural design and retrofit. *Monograph Series 1*, Multidisciplinary Center for Earthquake Engineering Research, Buffalo, NY, 1998.
10. Mokha AS, Constantinou MC, Reinhorn AM. Teflon bearing in base isolation. I: testing. *Journal of Structural Engineering* (ASCE) 1990; **116**:438–454.
11. Makris N, Chang S-P. Effect of viscous, viscoplastic and friction damping on the response of seismic isolated structures. *Earthquake Engineering and Structural Dynamics* 2000; **29**(1):85–107.
12. Makris N, Black CJ. Dimensional analysis of bilinear oscillators under pulse-type excitations. *Journal of Engineering Mechanics* (ASCE) 2004; **130**(9):1019–1031.
13. Hyakuda T, Saito K, Tanaka N, Yoneki S, Miyazaki M, Sawada T. The structural design and earthquake observation of a seismic isolated building using friction pendulum system. *Seventh International Seminar on Seismic Isolation*, *Passive Energy Dissipation and Active Control of Vibrations of Structures*, Assisi, Italy, 2–5/10, 2001.
14. Constantinou M. Friction pendulum double concave bearing. *Technical Report*, 2004. Available from: http://nees.buffalo.edu/docs/dec304/FP-DC%20Report-DEMO.pdf.
15. Tsai CS, Chiang TC, Chen BJ. Experimental evaluation piecewise exact solution for predicting seismic responses of spherical sliding type isolated structures. *Earthquake Engineering and Structural Dynamics* 2005; **34**(9):1027–1046.
16. Fenz DM, Constantinou MC. Behavior of the double concave Friction Pendulum bearing. *Earthquake Engineering and Structural Dynamics* 2006; **35**(11):1403–1424.
17. Tsai CS, Chen WS, Chiang TC, Chen BJ. Component and shaking table tests for full-scale multiple Friction Pendulum system. *Earthquake Engineering and Structural Dynamics* 2006; **35**(11):1653–1675.
18. Soni DP, Mistry BB, Jangid RS, Panchal VR. Seismic response of the double variable frequency pendulum isolator. *Structural Control and Health Monitoring* 2010; DOI: 101002/stc.384.
19. Chang SP, Makris N, Whittaker AS, Thompson ACT. Experimental and analytical studies on the performance of hybrid isolation systems. *Earthquake Engineering and Structural Dynamics* 2002; **31**(2):421–443.
20. Veletsos AS, Newmark NM, Chelepati CV. Deformation spectra for elastic and elastoplastic systems subjected to ground shock and earthquake motions. *Proceedings of the Third World Conference on Earthquake Engineering*, vol. II, Wellington, New Zealand, 1965; 663–682.
21. Hall JF, Heaton TH, Halling MW, Wald DJ. Near-source ground motion and its effects on flexible buildings. *Earthquake Spectra* 1995; **11**(4):569–605.
22. Heaton TH, Hall JF, Wald DJ, Halling MW. Response of high-rise and base-isolated buildings to a hypothetical Mw 7.0 blind thrust earthquake. *Science* 1995; **267**:206–211.
23. Makris N. Rigidity–plasticity–viscosity: can electrorheological dampers protect base-isolated structures from near-source ground motions? *Earthquake Engineering and Structural Dynamics* 1997; **26**:571–591.

24. Alavi B, Krawinkler H. Effects of near-source ground motions on frame-structures. *Technical Report No. 138*, The John A. Blume Earthquake Engineering Center, Stanford University, 2001.
25. Mavroeidis GP, Papageorgiou AS. A mathematical representation of near-fault ground motions. *Bulletin of the Seismological Society of America* 2003; **93**(3):1099–1131.
26. Aki K, Bouchon M, Chouet B, Das S. Quantitative prediction of strong motion for a potential earthquake fault. *Annali di Geofisica* 1977; **30**:341–368.
27. Papageorgiou AS, Aki K. A specific barrier model for the quantitative description of inhomogeneous faulting and the prediction of strong ground motion. II. Applications of the model. *Bulletin of the Seismological Society of America* 1983; **73**:953–978.
28. Brune JN. Tectonic stress and the spectra of seismic shear waves from earthquakes. *Journal of Geophysical Research* 1970; **75**:4997–5009.
29. Aki K. Strong-motion seismology. In *Earthquakes*: *Observation*, *Theory and Interpretation*, Kanamori H, Boschi E (eds). *Proceedings of the International School of Physics*, *Enrico Fermi*, *Course 85*. North-Holland: Amsterdam, 1983; 223–250.
30. Makris N, Black CJ. Dimensional analysis of rigid-plastic and elastoplastic structures under pulse-type excitations. *Journal of Engineering Mechanics* (ASCE) 2004; **130**(9):1006–1018.
31. Ricker N. Further developments in the wavelet theory of seismogram structure. *Bulletin of the Seismological Society of America* 1943; **33**:197–228.
32. Ricker N. Wavelet functions and their polynomials. *Geophysics* 1944; **9**:314–323.
33. Addison P. *The Illustrated Wavelet Transform Handbook*: *Introductory Theory and Applications in Science*, *Engineering*, *Medicine and Finance*. Institute of Physics: London, U.K., 2002.
34. Vassiliou MF, Makris N. Estimating time scales and length scales in earthquake acceleration records with the extended wavelet transform. *Report No. EEAM 2009-01*, University of Patras, Greece, 2009.
35. Barenblatt GI. *Scaling*, *Self-similarity*, *and Intermediate Asymptotics*. Cambridge University Press: Cambridge, U.K., 1996.
36. Kim YS, Yun CB. Seismic response characteristics of bridges using double concave friction pendulum bearings with tri-linear behaviour. *Engineering Structures* 2007; **29**(11):3082–3093.
37. Fenz DM, Constantinou MC. Spherical sliding isolation bearings with adaptive behavior: theory. *Earthquake Engineering and Structural Dynamics* 2008; **37**(2):163–183.
38. Zhang J, Makris N. Seismic response analysis of highway overcrossings including soil–structure interaction. *Earthquake Engineering and Structural Dynamics* 2002; **31**:1967–1991.

DOI: 10.1002/eqe